nature genetics

ANALYSIS

https://doi.org/10.1038/s41588-019-0516-6

Genome-wide association analysis of 19,629 individuals identifies variants influencing regional brain volumes and refines their genetic co-architecture with cognitive and mental health traits

Bingxin Zhao[1], Tianyou Luo[1], Tengfei Li[2,3], Yun Li[1,4,5], Jingwen Zhang[6], Yue Shan[1], Xifeng Wang[1], Liuqing Yang[7], Fan Zhou[1], Ziliang Zhu[1], Alzheimer's Disease Neuroimaging Initiative[8], Pediatric Imaging, Neurocognition and Genetics[8] and Hongtu Zhu[1,3*]

Volumetric variations of the human brain are heritable and are associated with many brain-related complex traits. Here we performed genome-wide association studies (GWAS) of 101 brain volumetric phenotypes using the UK Biobank sample including 19,629 participants. GWAS identified 365 independent genetic variants exceeding a significance threshold of 4.9×10^{-10}, adjusted for testing multiple phenotypes. A gene-based association study found 157 associated genes (124 new), and functional gene mapping analysis linked 146 additional genes. Many of the discovered genetic variants and genes have previously been implicated in cognitive and mental health traits. Through genome-wide polygenic-risk-score prediction, more than 6% of the phenotypic variance ($P = 3.13 \times 10^{-24}$) in four other independent studies could be explained by the UK Biobank GWAS results. In conclusion, our study identifies many new genetic associations at the variant, locus and gene levels and advances our understanding of the pleiotropy and genetic co-architecture between brain volumes and other traits.

Variations in regional brain volumes are heritable measures of brain functional and structural changes. Volumetric variations of the human brain are known to be phenotypically and genetically associated with heritable cognitive and mental health traits[1–5], and research is underway to understand the shared genetic influences on these traits[6]. Individual variations in the human brain volume are usually quantified by magnetic resonance imaging (MRI). In region of interest (ROI)-based analysis, whole-brain MRIs are processed and annotated onto many pre-defined ROIs, and then regional volumetric phenotypes are generated to measure the structure of brain ROIs. Both twin and population-based studies have shown that these volumetric phenotypes can be highly or moderately heritable. The heritability of brain regions estimated from twin studies can be larger than 80%[7–12]. For example, the heritability of basal ganglia structures (putamen, caudate and pallidum) and limbic and diencephalic regions (hippocampus, amygdala and thalamus) was reported to range from 0.60 to 0.85 (ref. [11]). Common genetic variants (typically SNPs) can account for more than 50% of the phenotypic variation in the general population[13–17]. The SNP heritability[18] estimates of the accumbens area, amygdala, putamen, palladium, caudate, thalamus and hippocampus range from 0.40 to 0.54 (ref. [15]). A highly polygenic or omnigenic[19,20] genetic architecture has been observed, which indicates that a large number of genetic variants influence regional brain volumes and their genetic contributions are widespread across the genome.

Several GWAS[3,14,17,21–25] have been conducted to identify genetic risk variants for brain volumetric phenotypes. However, except for the whole-brain volume and volumes of a few specific ROIs (for example, hippocampus in subcortical area[3,17,26]), GWAS of most brain volumetric phenotypes were insufficiently powered, for which the largest sample size of discovery GWAS was less than 10,000 in Elliott et al.[14]. Such GWAS sample size is much smaller than those of recent GWAS of other heritable brain-related traits, such as cognitive function[27], neuroticism[28] and intelligence[29], where sample sizes ranged from 269,867 to 449,484. Given the polygenic nature of brain volumes, most of the genetic risk variants may remain undetected, and GWAS with a larger sample size can uncover more associated variants and enrich the pleiotropy and genetic co-architecture with other traits. Recently, the UK Biobank (UKB[30]) study team has collected and released MRI data for more than 20,000 participants. In addition, publicly available imaging genetic datasets also emerge from several other independent studies, including the Philadelphia Neurodevelopmental Cohort (PNC[31]), the Alzheimer's Disease Neuroimaging Initiative (ADNI[32]), Pediatric Imaging, Neurocognition, and Genetics (PING[33]) and the Human Connectome Project (HCP[34]), among others. These datasets provide a new opportunity to perform better-powered GWAS of all ROI brain volumes.

Here we downloaded the raw MRI data from these data resources and processed the data using consistent standard procedures

[1]Department of Biostatistics, University of North Carolina at Chapel Hill, Chapel Hill, NC, USA. [2]Department of Radiology, University of North Carolina at Chapel Hill, Chapel Hill, NC, USA. [3]Biomedical Research Imaging Center, School of Medicine, University of North Carolina at Chapel Hill, Chapel Hill, NC, USA. [4]Department of Computer Science, University of North Carolina at Chapel Hill, Chapel Hill, NC, USA. [5]Department of Genetics, University of North Carolina at Chapel Hill, Chapel Hill, NC, USA. [6]Department of Biostatistics, T.H. Chan School of Public Health, Harvard University, Boston, MA, USA. [7]Department of Statistics and Operations Research, University of North Carolina at Chapel Hill, Chapel Hill, NC, USA. [8]A list of members and affiliations appears in the Supplementary Note. *e-mail: htzhu@email.unc.edu

via advanced normalization tools[35,36] to generate 101 regional (and total) brain volume phenotypes (referred to as ROI volumes), including total brain volume (TBV), gray matter, white matter and cerebrospinal fluid. We used 19,629 UKB individuals of British ancestry in the main discovery GWAS. Four other datasets with relatively small sample sizes (total sample size 2,192 after quality controls) were used to validate the UKB findings, and finally, a meta-analysis was performed to combine all of the data. We started our analysis of UKB data by estimating SNP heritability, which is the proportion of phenotypic variation that can be explained by the additive effects of all common autosomal variants[37]. Since the UKB MRI data were released at different time points, we organized them into two parts: the first part was released in 2017 (which we refer to as phase 1, $n=9{,}198$), most of which has been analyzed in Elliott et al.[14], and the second part was released in 2018 (which we refer to as phase 2, $n=10{,}431$). To detect any potential heterogeneity between the two phases, we compared the SNP heritability estimated in phase 2 data to that in phase 1 data. We then carried out GWAS to identify the associated genetic variants for each ROI volume. We performed gene-based association analysis via MAGMA[38] to uncover gene-level associations, and performed post-GWAS functional mapping and annotation (FUMA[39]) to explore the functional consequences of the significant genetic variants. We calculated the pairwise genetic correlation between ROI volumes and 50 brain-related complex traits by the linkage disequilibrium (LD) score regression (LDSC[40]). To confirm the robustness of UKB GWAS findings, we jointly analyzed the UKB GWAS results with those from PNC, ADNI, PING and HCP. We developed genome-wide polygenic risk scores (PRS) to assess the predictive ability of the UKB GWAS results on the four other datasets. GWAS summary statistics of the UKB sample and meta-analysis for the five studies have been made publicly available at https://github.com/BIG-S2/GWAS.

Results

SNP heritability estimates of the two UKB phases. In Supplementary Fig. 1, we compare the SNP heritability (h^2) estimated separately from UKB phase 1 and 2 data. The sample correlation coefficient of these estimates was 0.85 (correlation = 0.85), indicating a moderate to high level of agreement in terms of the degree of genetic contributions to ROI between the two phases. The mean h^2 across 101 ROI volumes was 0.41 for phase 1 and 0.37 for phase 2. The difference of mean h^2 was not significant (two-sided t-test, $P=0.12$). Ten ROIs had >0.6 h^2 estimates in both phases, including TBV, cerebellar vermal lobules VIII–X, cerebellar vermal lobules I–V, brain stem, left/right cerebellum exterior, left/right cerebellum white matter and left/right putamen. The h^2 estimates from the combined data were highly correlated with those from phase 1 (correlation = 0.93) and phase 2 (correlation = 0.95) (Supplementary Figs. 2 and 3). The h^2 and the corresponding 95% confidence interval (CI) are illustrated in Supplementary Figs. 4–6. The h^2 estimates, standard errors, and raw and Bonferroni-corrected P values from the one-sided likelihood ratio tests are provided in Supplementary Table 1. In the combined data, h^2 of most ROIs was significant after Bonferroni correction for multiple testing (mean $h^2=0.40$, h^2 range = (0.12, 0.72), standard error = 0.15). SNP heritability estimates of left basal forebrain ($h^2=0.10$) and optic chiasm ($h^2=0.06$) were not significant. These h^2 estimates were comparable with previous results[14,15]. In addition, for each ROI, we examined the genetic correlation of its regional volumes collected in the two phases. Genetic correlation estimates and the associated 95% CIs show a high degree of between-phase genetic similarity for most ROIs (Supplementary Table 1 and Supplementary Fig. 7). In summary, SNP heritability and genetic correlation analyses indicate that most ROI volumes are heritable and have a largely consistent genetic basis in the two phases' data.

Significant GWAS associations of 101 ROI volumes. We carried out GWAS of the 101 ROI volumes using 8,944,375 genetic variants after genotyping quality controls. Manhattan and quantile–quantile plots of all 101 phenotypes are displayed in Supplementary Datasets 1 and 2, respectively. In the rest of this paper, we use 4.9×10^{-10} (that is, $5\times10^{-8}/101$, additionally adjusted for all 101 GWAS performed) as the significance threshold for genetic variant-level associations unless otherwise stated.

We found that 365 independent significant variants had 494 significant associations with 58 ROIs (Supplementary Tables 2 and 3) at the 4.9×10^{-10} significance level. Independent significant variants were defined as significant variants that were independent of other significant variants by FUMA (Methods). The number of associations for each ROI is displayed in Fig. 1 and Supplementary Table 2. Left/right hippocampus, left/right putamen and cerebellar vermal lobules VIII–X had at least 30 independent significant variants. The number of independent significant associations on each chromosome is shown in Supplementary Table 4. Chromosome 12 had the largest number of independent variant-level associations after weighting by chromosome length (Supplementary Fig. 8).

Based on the pre-calculated LD structure from the 1000 Genomes reference panel[41], variants in LD with independent significant variants were identified and then (independent) lead variants and genetic risk loci were defined (Methods). The 494 independent significant variant-level associations were further characterized as 170 significant associations between genetic risk loci and ROI volumes (Supplementary Table 5). Brain stem, X4th ventricle, cerebellar vermal lobules VIII–X, cerebellar vermal lobules VI–VII, left/right putamen, left/right cerebellum exterior, left/right hippocampus, left/right lateral ventricle, left pallidum, TBV and white matter had at least five associated loci (Supplementary Table 2). Each chromosome had at least one associated locus except for chromosomes 13, 21 and 22 (Supplementary Table 6). Results at significance thresholds 5×10^{-8} and 5×10^{-9} are also provided in the above tables and summarized in Supplementary Table 7. We also performed association analysis for 283,120 genetic variants on the X chromosome (Methods) but observed no significant association at the 4.9×10^{-10} significance level.

Concordance with previous GWAS results. We performed association lookups for the 365 independent significant variants and their correlated variants in the NHGRI-EBI GWAS catalog[42]. We found that 166 independent significant variants (associated with 47 ROI volumes) have previously reported GWAS associations with other traits (Supplementary Table 8). Our results tagged many variants that were previously reported in GWAS of ROI volumes, including 19 variants in van der Meer et al.[3] for hippocampal subfield volumes, 12 in Hibar et al.[17] for subcortical brain region volumes, 6 in Chen et al.[43] for putamen volume, 4 in Bis et al.[25] for hippocampal volume, 2 in Hibar et al.[21] for hippocampal volume, 2 in Stein et al.[44] for brain structure, 2 in Ikram et al.[24] for intracranial volume, 1 in Furney et al.[45] for whole-brain volume and 1 in Baranzini et al.[46] for normalized brain volume (Supplementary Table 9). For the other traits, we highlighted previous associations of 46 variants with mental health disorders (such as schizophrenia, autism spectrum disorder and depression), 98 with cognitive functions, 25 with educational attainment, 24 with neuroticism, 14 with Parkinson's disease, 4 with reaction time and 3 with Alzheimer's disease. We observed more overlap with previous GWAS results when the significance threshold was relaxed to 5×10^{-8} (Supplementary Table 10). We also compared our results with those reported in Elliott et al.[14], who performed GWAS of 3,144 imaging phenotypes (including brain volume phenotypes processed by FreeSurfer[47]) using the UKB phase 1 data ($n=8{,}428$). When both were corrected for the number of GWAS analyses performed, 26 of the 78 significant variants reported in Elliott et al.[14] were in LD ($r^2\geq0.6$) with our independent significant variants

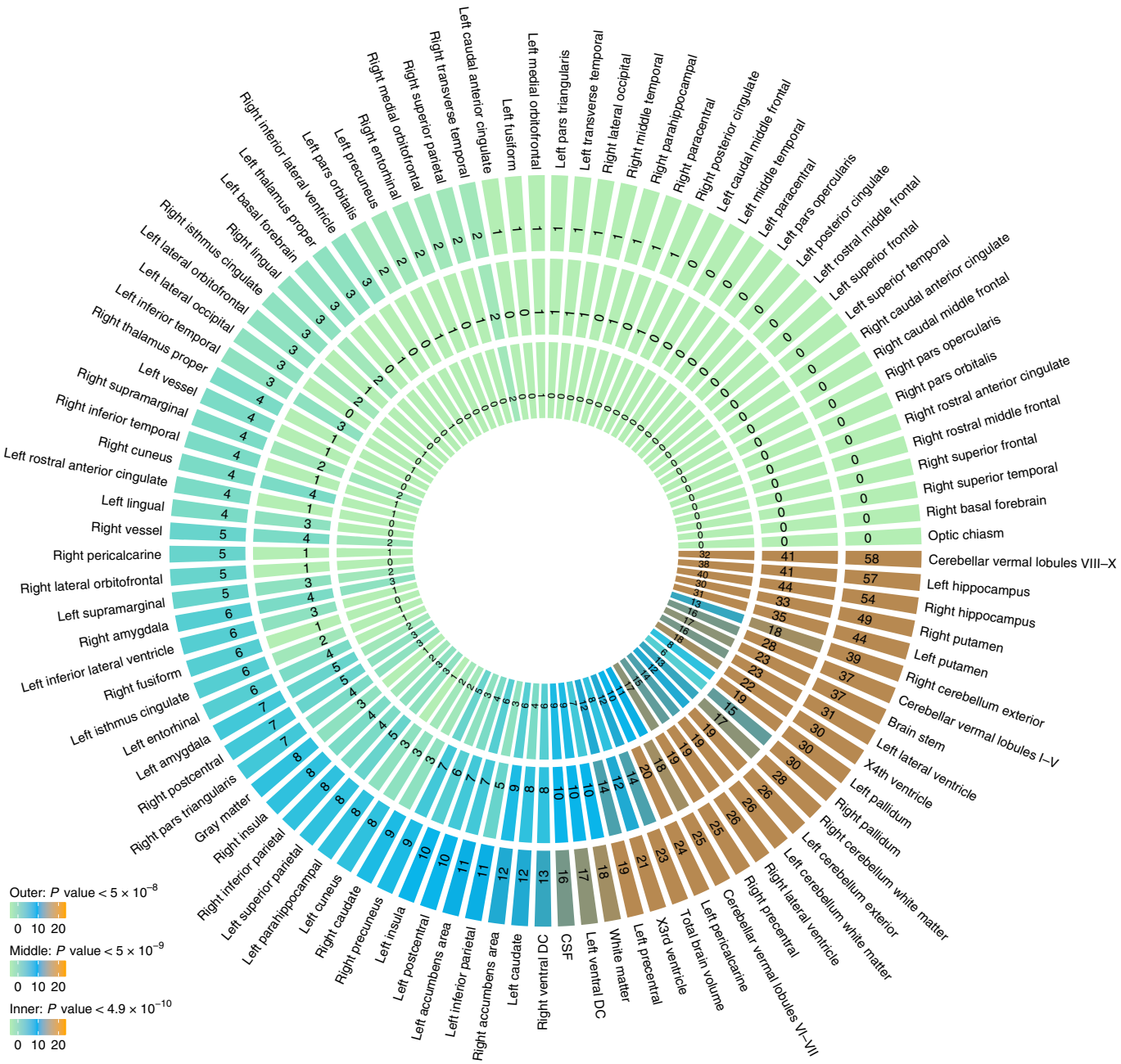

Fig. 1 | The number of independent significant variant-level associations discovered in UKB GWAS ($n = 19{,}629$ subjects) at different significance levels. The P values are raw P values of two-sided t-test statistics. The outer layer counts the number of associations for each ROI volume with $P < 5 \times 10^{-8}$, the middle layer counts the ones with $P < 5 \times 10^{-9}$, and the inner layer counts those with $P < 4.9 \times 10^{-10}$. The 4.9×10^{-10} threshold corresponds to adjusting for testing multiple imaging phenotypes with Bonferroni correction. DC, diencephalon.

(Supplementary Table 11). When both were relaxed to the 5×10^{-8} significance threshold, 124 of their 616 significant variants were in LD with our independent significant variants.

Gene-based association analysis and functional mapping. We performed gene-based association analysis with GWAS summary statistics for 18,796 candidate genes (Methods). We found 281 significant gene-level associations ($P < 2 \times 10^{-8}$, adjusted for multiple traits) between 157 genes and 55 ROIs (Supplementary Table 12). Our results replicated 33 genes discovered in previous studies, including *FOXO3* in Baranzini et al.[46] for normalized brain volume, *GATAD2B* in Hibar et al.[48] for lentiform nucleus volume, *GNA12* in Sprooten et al.[49] for white matter integrity, *MCC* in Kim and Webster[50] for brain cytoarchitecture, *HMGA2* and *HRK* in Stein et al.[44] for brain structure, *KANSL1*, *MAPT*, *STH* and *CENPW* in Ikram et al.[24] for intracranial volume, *GMNC*, *WNT3* and *PDCD11* in Klein et al.[51] for intracranial volume, *SLC44A5* in Furney et al.[45] for whole-brain volume, *MSRB3*, *BCL2L1*, *DCC* and *CRHR1* in Hibar et al.[17] for subcortical brain region volumes, *LEMD3*, *WIF1* and *ASTN2* in Bis et al.[25] for hippocampal volume, *MAST4*, *FAM53B*, *METTL10* and *FAF1* in van der Meer et al.[3] for hippocampal subfield volumes, *DSCAML1* and *KTN1* in Chen et al.[43] for putamen volume, and *ZIC4*, *VCAN*, *PAPPA*, *DRAM1*, *DAAM1* and *ALDH1A2* in Elliott et al.[14] for brain imaging measurements. We found that 124 genes were novel and had not been linked to ROI volumes previously (Supplementary Table 13). Of the 157 detected

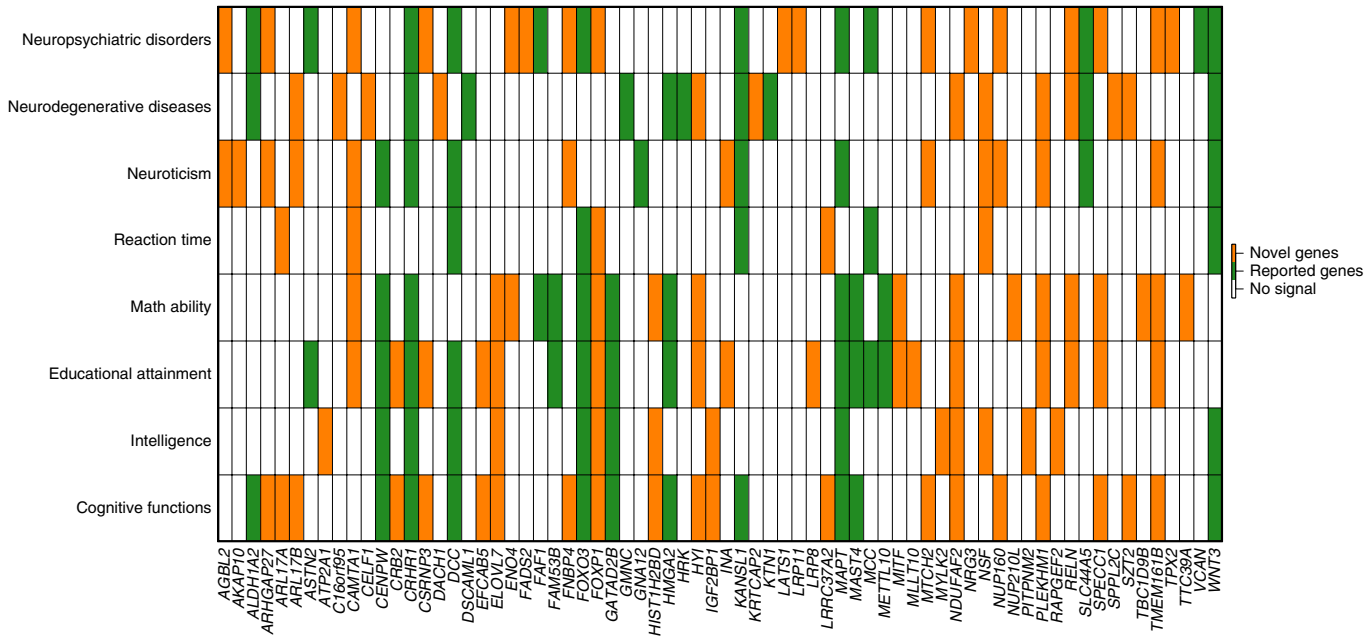

Fig. 2 | Genes identified in gene-based association analysis of ROI volumes ($n = 19,629$ subjects) that have been linked to cognitive traits and mental health disorders in previous GWAS. For each of the ROI-associated genes listed in the *x* axis, we manually checked the previously reported associations in the NHGRI-EBI GWAS catalog (https://www.ebi.ac.uk/gwas/). The novel and previously reported genes of ROI volumes were labeled with two different colors (orange and green, respectively).

genes, 70 have previously been implicated in cognitive functions, intelligence, education, neuroticism, and neuropsychiatric and neurodegenerative diseases/disorders, such as *IGF2BP1* (refs. [29,52]), *WNT3* (refs. [27,28,53,54]), *PLEKHM*[54–56] and *AGBL2* (refs. [28,54,57,58]). In particular, 47 of the 70 pleiotropic genes were novel genes of ROI volumes, and thus these findings substantially uncovered the gene-level pleiotropy between ROI volumes and these traits (Fig. 2).

The independent significant variants were also annotated by functional consequences on gene functions (Supplementary Table 14 and Supplementary Fig. 9), and were subsequently mapped to genes according to physical position, expression quantitative trait loci (eQTL) association (for brain tissues) and three-dimensional chromatin (Hi-C) interaction (Methods). Functional gene mapping yielded 505 significant associations for 279 genes and 53 ROIs (Supplementary Table 15). Of the 279 genes, 163 were not discovered in the above gene-based association analysis, which replicated more previous findings on ROI volumes, such as *FBXW8* in Stein et al.[44] for brain structure, *WNT16* in Zheng et al.[59] for cortical thickness, *TBPL2* in Chen et al.[43] for putamen volume, *FAT3* in Hibar et al.[17] for subcortical brain region volumes, *FAM175B*, *LHPP*, *SLC4A10*, *RNFT2*, *TESC*, *FOXD2*, *DMRTA2*, *CDKN2C* and *DPP4* in van der Meer et al.[3] for hippocampal subfield volumes, and *EPHA3*, *SLC39A8*, *BANK1*, *CHPT1*, *ACADM*, *FAM3C*, *L3HYPDH*, *JKAMP* and *AQP9* in Elliott et al.[14] for brain imaging measurements. We found that 53 (41 new) of the 163 genes were associated with cognitive functions, intelligence, education, neuroticism, neuropsychiatric and neurodegenerative disorders, such as *NT5C2* (refs. [28,55,60,61]), *ADAM10* (refs. [61,62]) and *GOSR1* (refs. [27,55]) (Supplementary Fig. 10). In particular, 182 significant Hi-C interactions were observed in the Hi-C functional mapping analysis (Supplementary Table 16), which yielded 33 significant associations between 13 genes and 16 ROIs (Supplementary Table 17). Of the 13 genes, 5 were not mapped by physical position or eQTL association, such as *C5orf64* for left pericalcarine. *C5orf64* has been reported to be associated with cognitive functions and intelligence[27], education and math ability[55], as well as risk behaviors[63] and Alzheimer's disease[64].

In addition, we explored the biological interpretations of our GWAS results by performing several enrichment and annotation analyses, including gene property analysis by MAGMA and chromatin-based annotation analysis by stratified LDSC[65] (Methods). To gain more insights into the biological mechanisms, we used DEPICT[66] and MAGMA to conduct gene set analysis (Methods). The results can be found in Supplementary Note and are summarized in Supplementary Tables 18–21. In general, although some positive results can be obtained from these analyses, the present GWAS still has limited power to infer the specific biological pathway(s) influencing brain ROI volumes, and future GWAS with a larger sample size is needed to further explore the biological mechanisms of brain imaging phenotypes.

Joint analysis with four independent datasets. To validate the UKB GWAS results, we repeated GWAS of 101 ROI volumes separately on data obtained from four other independent studies: PNC ($n = 537$), HCP ($n = 334$), PING ($n = 461$) and ADNI ($n = 860$). Due to the small sample size of these four datasets, the probability of replicating significant findings in the UKB was low. Instead, we checked whether the effect signs were concordant in the five studies and whether the *P* value of the top UKB risk variants decreased after meta-analysis (Methods). Smaller *P* values after meta-analysis indicate similar variant effects in independent samples[67,68].

We carried out a joint analysis on 3,841,911 genetic variants that were present in all five sets of GWAS results. For the 7,310 significant associations (at the 4.9×10^{-10} significance level), 63.8% (4,666) associations had the same effect signs across the five studies, and 97.0% (7,090) associations had the same effect signs in at least four studies (including UKB). Specifically, the number of genetic variants that had the same effect sign as UKB was 6,823 (93.3%) for ADNI, 6,436 (88.0%) for HCP, 6,455 (88.3%) for PING and 6,648 (91.0%) for PNC. An exact binomial test[69] showed a significant non-random agreement in effect signs across all of the four studies (one-sided $P < 2.2 \times 10^{-16}$, null hypothesis: agreement has a probability 0.5). Of the top 2,000 significant associations, 93.9% (1,877) had a

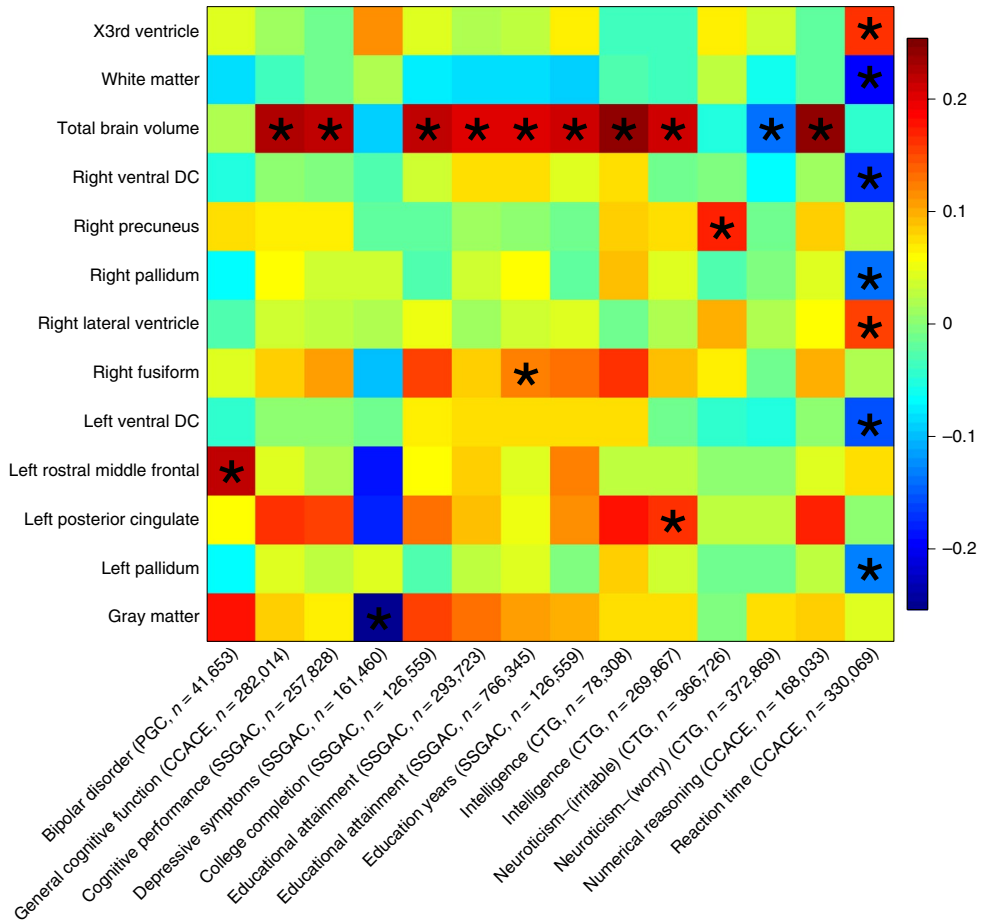

Fig. 3 | Selected pairwise genetic correlations between ROI volumes ($n = 21,821$ subjects) and other traits. The pairwise genetic correlations were estimated and tested by LDSC (https://github.com/bulik/ldsc). The asterisks highlight significant associations after adjusting for multiple testing by the Benjamini–Hochberg procedure at the 0.05 significance level. The *y* axis lists the ROI volumes. The *x* axis provides the name of cognitive or mental health traits, the consortium sharing the GWAS summary statistics and the corresponding sample sizes (see Supplementary Table 24 for further information about these studies).

smaller *P* value after meta-analysis, and 91.4% (6,678) of the 7,310 associations were enhanced. We then performed meta-analysis on all 8,944,375 UKB GWAS genetic variants (variants were allowed to be missing in the four independent datasets). Compared to the UKB GWAS results (Supplementary Table 2, Supplementary Fig. 11 and Supplementary Note), there were more significant associations after meta-analysis: 29,585 significant associations at the 5×10^{-8} significance level and 16,591 at the 4.9×10^{-10} significance level (Supplementary Table 22 and Supplementary Fig. 12).

Genetic correlation with other traits. We used the meta-analysis GWAS results to estimate the genetic correlation with other traits via LDSC. As positive controls, we first estimated the genetic correlation between several UKB ROI volumes (TBV, left/right thalamus proper, left/right caudate, left/right putamen, left/right pallidum, left/right hippocampus and left/right accumbens area) and their corresponding traits studied in the ENIGMA consortium[70]. The genetic correlation estimates were all significant ($P < 4.13 \times 10^{-6}$), and the average correlation was 0.95 (Supplementary Table 23). We then collected 50 sets of publicly available GWAS summary statistics (Supplementary Table 24) and calculated their pairwise genetic correlation with ROI volumes (Supplementary Table 25). We mainly focused on traits that showed evidence of pleiotropy in association lookups. There were 22 significant associations after adjusting for multiple testing by the Benjamini–Hochberg procedure at the 0.05 level (Supplementary Table 26 and Supplementary Fig. 13).

Significant genetic correlations linked 13 ROI volumes with general cognitive functions, education (education years, college completion), intelligence, numerical reasoning, reaction time, depressive symptoms, neuroticism and bipolar disorder (Fig. 3), which matched our findings in variant- and gene-level lookups. In particular, TBV had positive correlations with cognitive functions, education, intelligence and numerical reasoning (genetic correlation range = (0.20, 0.25), mean = 0.22, *P*-value range = (1.52×10^{-11}, 3.45×10^{-5})). These results matched the previous finding that brain size has small but significant connections with cognitive performance[71]. Reaction time had negative correlations with left/right pallidum, left/right ventral diencephalon and white matter (genetic correlation range = (−0.20, −0.13), *P*-value range = (3.80×10^{-7}, 1.14×10^{-4})). The negative correlations between reaction time and white matter volumes have previously been reported[72,73]. Further details can be found in the Supplementary Note. When the false discover rate level was relaxed to 0.1, suggestive evidence was observed for more brain-related traits, such as autism spectrum disorder and sleep traits (Supplementary Table 26 and Supplementary Fig. 14). In conclusion, our results confirm the significant genetic correlation among these traits and quantify the degree of their genetic overlaps.

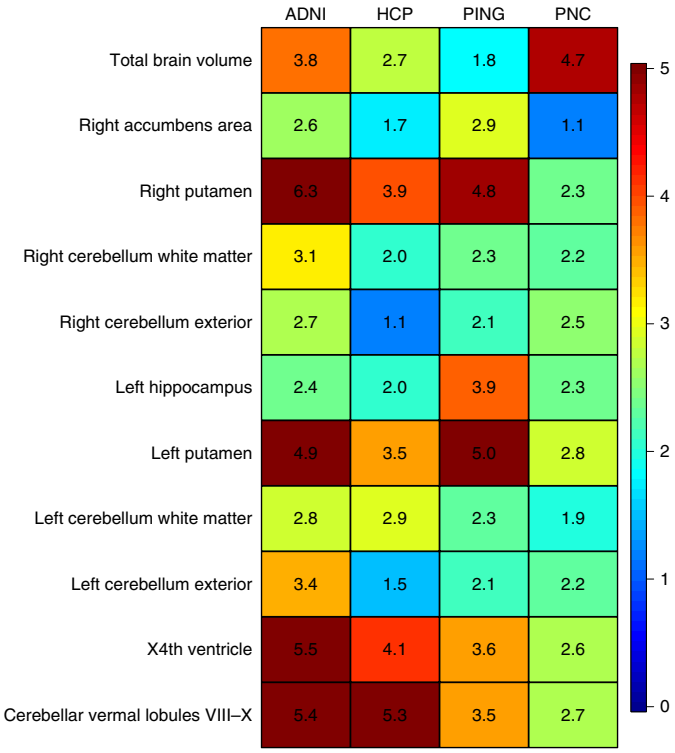

Fig. 4 | Prediction accuracy (incremental R-squared) of PRSs constructed by UKB GWAS ($n = 19{,}629$ subjects) summary statistics on the four independent datasets. The *y* axis lists the ROI volumes (left/right cerebellum exterior, left/right putamen, left/right cerebellum white matter, left hippocampus, cerebellar vermal lobules VIII–X, X4th ventricle, right accumbens area and TBV). The *x* axis lists the four independent cohorts (ADNI, HCP, PING and PNC). The displayed numbers are the proportions of phenotypic variation that can be additionally explained by PRSs (that is, the incremental *R*-squared; see Methods for details of polygenic risk prediction).

Predictive ability of the UKB GWAS results. We examined the out-of-sample prediction power of the UKB GWAS summary statistics using PRS prediction[74]. We first used a tenfold cross-validation design to examine the prediction power within the UKB sample for seven ROIs, including the thalamus proper, caudate, putamen, pallidum, hippocampus, accumbens area and TBV (Methods). The polygenic profiles can explain 1.18%–3.93% of the phenotypic variance (P-value range = (7.88×10^{-210}, 4.90×10^{-72})) for these ROIs. The largest R-squared of 3.93% was observed on putamen. Next, we used ROI-derived profiles to carry out cross-trait prediction on brain-related traits including education, reaction time, numeric memory and fluid intelligence. The largest R-squared of a single profile was 0.24% ($P = 7.53 \times 10^{-7}$), which occurred when using the TBV-derived profile to predict fluid intelligence. When putting the profiles of seven ROIs together in one multivariate model, the R-squared for predicting fluid intelligence can be improved to 0.52% ($P = 1.89 \times 10^{-9}$). These results are summarized in Supplementary Table 27.

We then used the GWAS summary statistics of 19,629 UKB individuals to construct polygenic profiles on subjects in PNC, HCP, PING and ADNI. We found that, for 11 ROIs (Fig. 4), the genetically predicted regional volume was significantly associated with the observed ROI volume in all four validation datasets after Bonferroni correction (that is, $101 \times 4 = 404$ tests), and can account for 1.17%–6.38% of the phenotypic variance (P-value range = (3.31×10^{-24}, 1.68×10^{-5})) (Supplementary Table 28). For example, the R-squared of the right putamen-derived profile was 6.38% in ADNI and 4.85% in PNC. Furthermore, 29 genetically predicted regional volumes were significant in at least three of the four datasets, 56 in at least two datasets, and 84 in at least one dataset (Supplementary Figs. 15–17). In summary, our within-UKB and out-of-UKB PRS analyses clearly indicate that UKB GWAS summary statistics of ROI volumes have widespread prediction power across ROIs. However, the R-squared can be low when predicting other brain-related complex traits. Such results are unsurprising because the genetic correlations among these traits were found to be small (although significant) in LDSC analysis.

Discussion

In this study, we presented GWAS of 101 ROI volumes using data for 19,629 UKB individuals. Our novel contributions include: identification of many new genetic associations at the variant, locus and gene levels; insights into the genetic co-architecture of brain volume phenotypes and other brain-related complex traits; validation of the UKB results in independent studies; and assessment of the predictive power of UKB GWAS results. Significant ($P < 4.9 \times 10^{-10}$) associations were found for 58 of the 101 ROIs. With a larger sample size, the present study replicated many known genetic variants but also prioritized new ones. Compared to Elliott et al.[14], our GWAS not only discovered more genetic variants, but also enriched the degree of (statistical) pleiotropy[75] of the associated genes and characterized the shared genetic influences with cognitive and mental health traits. Our SNP heritability estimates are aligned with the previous results of existing twin studies. For example, our results supported previous findings that the degree of genetic control varies across different regions within the brain[7,12,76,77]. We also confirmed that cortical ROIs have larger variability in their heritability estimates than subcortical and ventricular ROIs[11]. In addition, some subcortical ROIs, such as putamen, cerebellum white matter and brain stem[11,78], were confirmatively highly heritable. On the other hand, SNP heritability of ROI volumes was found to be generally lower than estimates reported in twin studies[7–10]. This is expected[79] and may indicate that genetic influences cannot be fully captured by additive effects of common genetic variants[37]. Such gaps may inspire future work to explore the effects of rare genetic variants on ROI volumes and to better model the genetic variation of the brain.

The present GWAS still faces some limitations. First, the current GWAS sample size of ROI volumes (and many other brain imaging phenotypes) is still far from sufficient. The highly polygenic genetic architecture of ROI volumes requires a larger number of individuals to identify many weak causal variants. In the era of sharing GWAS summary statistics, well-powered GWAS are essential to study the genetic co-architecture among complex traits. For example, a recent study by Watanabe et al.[75] to discover the global overview of the genetic co-architecture of 2,965 traits focused only on GWAS with a sample size larger than 50,000, with the average sample size of selected traits being 256,276. In our genetic correlation analysis, we obtained only a limited number of significant correlations, even though many pleiotropic genes were found in association lookups. In addition, ROI-derived PRS currently may have insufficient power to predict other brain-related traits. Therefore, we expect that GWAS of ROI volumes with a larger sample size will be available and can further improve our understanding of genetic overlaps underlying other traits. Besides increasing the sample size, combining genotyping data with external information, such as gene expression data[80], may also help elucidate causal mechanisms, improve prediction performance and identify genetic connections among traits.

Second, potential imaging artifacts, such as MRI hardware and software changes[81], may cause unwanted variation in downstream genetic analyses, especially when combining multi-site and multiple-phase neuroimaging data[82–84]. In the present GWAS, we confirmed that the UKB phase 1 and 2 data have a largely consistent genetic basis, and verified that the UKB GWAS results had satisfactory

prediction ability on four other independent datasets. However, we found that the SNP heritability estimates of the two phases data were not perfectly harmonized. The inadequate GWAS sample size may partially explain the variation in these heritability estimates, but it is also possible that artificial factors impaired the consistency of our results (see Table 1 of Smith and Nichols[82] for a list of common imaging batch effects). Future studies that integrate data from more sites and phases are expected to be batch effects-aware and to confirm the previous GWAS findings.

Online content

Any methods, additional references, Nature Research reporting summaries, source data, extended data, supplementary information, acknowledgements, peer review information; details of author contributions and competing interests; and statements of data and code availability are available at https://doi.org/10.1038/s41588-019-0516-6.

Received: 24 March 2019; Accepted: 23 September 2019;
Published online: 1 November 2019

References

1. Ritchie, S. J. et al. Beyond a bigger brain: multivariable structural brain imaging and intelligence. *Intelligence* **51**, 47–56 (2015).
2. Davies, G. et al. Genome-wide association study of cognitive functions and educational attainment in UK Biobank (N=112 151). *Mol. Psychiatry* **21**, 758–767 (2016).
3. van der Meer, D. et al. Brain scans from 21,297 individuals reveal the genetic architecture of hippocampal subfield volumes. *Mol. Psychiatry* https://doi.org/10.1038/s41380-018-0262-7 (2018).
4. Caldiroli, A. et al. The relationship of IQ and emotional processing with insula volume in schizophrenia. *Schizophrenia Res.* **202**, 141–148 (2018).
5. Vreeker, A. et al. The relationship between brain volumes and intelligence in bipolar disorder. *J. Affect. Disord.* **223**, 59–64 (2017).
6. Wigmore, E. M. et al. Do regional brain volumes and major depressive disorder share genetic architecture? A study of Generation Scotland (*n*=19 762), UK Biobank (*n*= 24 048) and the English Longitudinal Study of Ageing (*n*=5766). *Transl. Psychiatry* **7**, e1205 (2017).
7. Wen, W. et al. Distinct genetic influences on cortical and subcortical brain structures. *Sci. Rep.* **6**, 32760 (2016).
8. den Braber, A. et al. Heritability of subcortical brain measures: a perspective for future genome-wide association studies. *NeuroImage* **83**, 98–102 (2013).
9. Eyler, L. T. et al. Conceptual and data-based investigation of genetic influences and brain asymmetry: a twin study of multiple structural phenotypes. *J. Cogn. Neurosci.* **26**, 1100–1117 (2014).
10. Blokland, G. A., de Zubicaray, G. I., McMahon, K. L. & Wright, M. J. Genetic and environmental influences on neuroimaging phenotypes: a meta-analytical perspective on twin imaging studies. *Twin Res. Hum. Genet.* **15**, 351–371 (2012).
11. Kremen, W. S. et al. Genetic and environmental influences on the size of specific brain regions in midlife: the VETSA MRI study. *NeuroImage* **49**, 1213–1223 (2010).
12. Jansen, A. G., Mous, S. E., White, T., Posthuma, D. & Polderman, T. J. What twin studies tell us about the heritability of brain development, morphology, and function: a review. *Neuropsychol. Rev.* **25**, 27–46 (2015).
13. Zhao, B. et al. Heritability of regional brain volumes in large-scale neuroimaging and genetic studies. *Cereb. Cortex* **29**, 2904–2914 (2018).
14. Elliott, L. T. et al. Genome-wide association studies of brain imaging phenotypes in UK Biobank. *Nature* **562**, 210–216 (2018).
15. Biton, A. et al. Polygenic architecture of human neuroanatomical diversity. Preprint at *bioRxiv* https://doi.org/10.1101/592337 (2019).
16. Toro, R. et al. Genomic architecture of human neuroanatomical diversity. *Mol. Psychiatry* **20**, 1011–1016 (2015).
17. Hibar, D. P. et al. Common genetic variants influence human subcortical brain structures. *Nature* **520**, 224–229 (2015).
18. Yang, J. et al. Common SNPs explain a large proportion of the heritability for human height. *Nat. Genet.* **42**, 565–569 (2010).
19. Boyle, E. A., Li, Y. I. & Pritchard, J. K. An expanded view of complex traits: from polygenic to omnigenic. *Cell* **169**, 1177–1186 (2017).
20. Timpson, N. J., Greenwood, C. M. T., Soranzo, N., Lawson, D. J. & Richards, J. B. Genetic architecture: the shape of the genetic contribution to human traits and disease. *Nat. Rev. Genet.* **19**, 110–124 (2017).
21. Hibar, D. P. et al. Novel genetic loci associated with hippocampal volume. *Nat. Commun.* **8**, 13624 (2017).
22. Franke, B. et al. Genetic influences on schizophrenia and subcortical brain volumes: large-scale proof of concept. *Nat. Neurosci.* **19**, 420–431 (2016).
23. Guadalupe, T. et al. Human subcortical brain asymmetries in 15,847 people worldwide reveal effects of age and sex. *Brain Imaging Behav.* **11**, 1497–1514 (2017).
24. Ikram, M. A. et al. Common variants at 6q22 and 17q21 are associated with intracranial volume. *Nat. Genet.* **44**, 539–544 (2012).
25. Bis, J. C. et al. Common variants at 12q14 and 12q24 are associated with hippocampal volume. *Nat. Genet.* **44**, 545–551 (2012).
26. Satizabal, C. L. et al. Genetic architecture of subcortical brain structures in over 40,000 individuals worldwide. Preprint at *bioRxiv* https://doi.org/10.1101/173831 (2017).
27. Davies, G. et al. Study of 300,486 individuals identifies 148 independent genetic loci influencing general cognitive function. *Nat. Commun.* **9**, 2098 (2018).
28. Nagel, M. et al. Meta-analysis of genome-wide association studies for neuroticism in 449,484 individuals identifies novel genetic loci and pathways. *Nat. Genet.* **50**, 920–927 (2018).
29. Savage, J. E. et al. Genome-wide association meta-analysis in 269,867 individuals identifies new genetic and functional links to intelligence. *Nat. Genet.* **50**, 912–919 (2018).
30. Sudlow, C. et al. UK Biobank: an open access resource for identifying the causes of a wide range of complex diseases of middle and old age. *PLoS Med.* **12**, e1001779 (2015).
31. Satterthwaite, T. D. et al. Neuroimaging of the Philadelphia neurodevelopmental cohort. *Neuroimage* **86**, 544–553 (2014).
32. Weiner, M. W. et al. The Alzheimer's Disease Neuroimaging Initiative: a review of papers published since its inception. *Alzheimer's Dement.* **9**, e111–e194 (2013).
33. Jernigan, T. L. et al. The Pediatric Imaging, Neurocognition, and Genetics (PING) data repository. *Neuroimage* **124**, 1149–1154 (2016).
34. Somerville, L. H. et al. The Lifespan Human Connectome Project in Development: a large-scale study of brain connectivity development in 5–21 year olds. *NeuroImage* **183**, 456–468 (2018).
35. Avants, B. B. et al. A reproducible evaluation of ANTs similarity metric performance in brain image registration. *NeuroImage* **54**, 2033–2044 (2011).
36. Tustison, N. J. et al. Large-scale evaluation of ANTs and FreeSurfer cortical thickness measurements. *NeuroImage* **99**, 166–179 (2014).
37. Yang, J., Zeng, J., Goddard, M. E., Wray, N. R. & Visscher, P. M. Concepts, estimation and interpretation of SNP-based heritability. *Nat. Genet.* **49**, 1304–1310 (2017).
38. de Leeuw, C. A., Mooij, J. M., Heskes, T. & Posthuma, D. MAGMA: generalized gene-set analysis of GWAS data. *PLoS Computational Biol.* **11**, e1004219 (2015).
39. Watanabe, K., Taskesen, E., Bochoven, A. & Posthuma, D. Functional mapping and annotation of genetic associations with FUMA. *Nat. Commun.* **8**, 1826 (2017).
40. Bulik-Sullivan, B. et al. An atlas of genetic correlations across human diseases and traits. *Nat. Genet.* **47**, 1236–1241 (2015).
41. 1000 Genomes Project Consortium A global reference for human genetic variation. *Nature* **526**, 68–74 (2015).
42. Buniello, A. et al. The NHGRI-EBI GWAS Catalog of published genome-wide association studies, targeted arrays and summary statistics 2019. *Nucleic Acids Res.* **47**, D1005–D1012 (2018).
43. Chen, C.-H. et al. Leveraging genome characteristics to improve gene discovery for putamen subcortical brain structure. *Sci. Rep.* **7**, 15736 (2017).
44. Stein, J. L. et al. Identification of common variants associated with human hippocampal and intracranial volumes. *Nat. Genet.* **44**, 552–561 (2012).
45. Furney, S. et al. Genome-wide association with MRI atrophy measures as a quantitative trait locus for Alzheimer's disease. *Mol. Psychiatry* **16**, 1130–1138 (2011).
46. Baranzini, S. E. et al. Genome-wide association analysis of susceptibility and clinical phenotype in multiple sclerosis. *Hum. Mol. Genet.* **18**, 767–778 (2008).
47. Fischl, B. FreeSurfer. *NeuroImage* **62**, 774–781 (2012).
48. Hibar, D. P. et al. Genome-wide association identifies genetic variants associated with lentiform nucleus volume in N=1345 young and elderly subjects. *Brain Imaging Behav.* **7**, 102–115 (2013).
49. Sprooten, E. et al. White matter integrity as an intermediate phenotype: exploratory genome-wide association analysis in individuals at high risk of bipolar disorder. *Psychiatry Res.* **206**, 223–231 (2013).
50. Kim, S. & Webster, M. Integrative genome-wide association analysis of cytoarchitectural abnormalities in the prefrontal cortex of psychiatric disorders. *Mol. Psychiatry* **16**, 452–461 (2011).
51. Klein, M. et al. Genetic markers of ADHD-related variations in intracranial volume. *Am. J. Psychiatry* **176**, 228–238 (2019).
52. Hill, W. et al. A combined analysis of genetically correlated traits identifies 187 loci and a role for neurogenesis and myelination in intelligence. *Mol. Psychiatry* **24**, 169–181 (2019).
53. Jun, G. et al. A novel Alzheimer disease locus located near the gene encoding tau protein. *Mol. Psychiatry* **21**, 108–117 (2016).

54. Luciano, M. et al. Association analysis in over 329,000 individuals identifies 116 independent variants influencing neuroticism. *Nat. Genet.* **50**, 6–11 (2018).
55. Lee, J. J. et al. Gene discovery and polygenic prediction from a genome-wide association study of educational attainment in 1.1 million individuals. *Nat. Genet.* **50**, 1112–1121 (2018).
56. Edwards, T. L. et al. Genome-wide association study confirms SNPs in SNCA and the MAPT region as common risk factors for Parkinson disease. *Ann. Hum. Genet.* **74**, 97–109 (2010).
57. Turley, P. et al. Multi-trait analysis of genome-wide association summary statistics using MTAG. *Nat. Genet.* **50**, 229–237 (2018).
58. Okbay, A. et al. Genetic variants associated with subjective well-being, depressive symptoms, and neuroticism identified through genome-wide analyses. *Nat. Genet.* **48**, 624–633 (2016).
59. Zheng, H.-F. et al. WNT16 influences bone mineral density, cortical bone thickness, bone strength, and osteoporotic fracture risk. *PLoS Genet.* **8**, e1002745 (2012).
60. Pardiñas, A. F. et al. Common schizophrenia alleles are enriched in mutation-intolerant genes and in regions under strong background selection. *Nat. Genet.* **50**, 381–389 (2018).
61. Li, Z. et al. Genome-wide association analysis identifies 30 new susceptibility loci for schizophrenia. *Nat. Genet.* **49**, 1576–1583 (2017).
62. Marioni, R. E. et al. GWAS on family history of Alzheimer's disease. *Transl. Psychiatry* **8**, 99 (2018).
63. Linnér, R. K. et al. Genome-wide association analyses of risk tolerance and risky behaviors in over 1 million individuals identify hundreds of loci and shared genetic influences. *Nat. Genet.* **51**, 245–257 (2019).
64. Kamboh, M. et al. Genome-wide association study of Alzheimer's disease. *Transl. Psychiatry* **2**, e117 (2012).
65. Finucane, H. K. et al. Heritability enrichment of specifically expressed genes identifies disease-relevant tissues and cell types. *Nat. Genet.* **50**, 621–629 (2018).
66. Pers, T. H. et al. Biological interpretation of genome-wide association studies using predicted gene functions. *Nat. Commun.* **6**, 5890 (2015).
67. Jansen, P. R. et al. Genome-wide analysis of insomnia in 1,331,010 individuals identifies new risk loci and functional pathways. *Nat. Genet.* **51**, 394–403 (2019).
68. Skol, A. D., Scott, L. J., Abecasis, G. R. & Boehnke, M. Joint analysis is more efficient than replication-based analysis for two-stage genome-wide association studies. *Nat. Genet.* **38**, 209–213 (2006).
69. Hanscombe, K. B. et al. Genetic factors influencing coagulation factor XIII B-subunit contribute to risk of ischemic stroke. *Stroke* **46**, 2069–2074 (2015).
70. Thompson, P. M. et al. The ENIGMA consortium: large-scale collaborative analyses of neuroimaging and genetic data. *Brain Imaging Behav.* **8**, 153–182 (2014).
71. Nave, G., Jung, W. H., Karlsson Linnér, R., Kable, J. W. & Koellinger, P. D. Are bigger brains smarter? Evidence from a large-scale preregistered study. *Psychological Sci.* **30**, 43–54 (2019).
72. Walhovd, K. B. & Fjell, A. M. White matter volume predicts reaction time instability. *Neuropsychologia* **45**, 2277–2284 (2007).
73. Delorme, S. et al. Reaction time is negatively associated with corpus callosum area in the early stages of CADASIL. *Am. J. Neuroradiol.* **38**, 2094–2099 (2017).
74. The International Schizophrenia Consortium Common polygenic variation contributes to risk of schizophrenia and bipolar disorder. *Nature* **460**, 748–752 (2009).
75. Watanabe, K. et al. A global overview of pleiotropy and genetic architecture in complex traits. *Nat. Genet.* **51**, 1339–1348 (2019).
76. Thompson, P. M. et al. Genetic influences on brain structure. *Nat. Neurosci.* **4**, 1253–1258 (2001).
77. Peper, J. S., Brouwer, R. M., Boomsma, D. I., Kahn, R. S. & Hulshoff Pol, H. E. Genetic influences on human brain structure: a review of brain imaging studies in twins. *Hum. Brain Mapp.* **28**, 464–473 (2007).
78. Yoon, U., Perusse, D., Lee, J.-M. & Evans, A. C. Genetic and environmental influences on structural variability of the brain in pediatric twin: deformation based morphometry. *Neurosci. Lett.* **493**, 8–13 (2011).
79. Manolio, T. A. et al. Finding the missing heritability of complex diseases. *Nature* **461**, 747–753 (2009).
80. Gusev, A. et al. Transcriptome-wide association study of schizophrenia and chromatin activity yields mechanistic disease insights. *Nat. Genet.* **50**, 538–548 (2018).
81. Miller, K. L. et al. Multimodal population brain imaging in the UK Biobank prospective epidemiological study. *Nat. Neurosci.* **19**, 1523–1536 (2016).
82. Smith, S. M. & Nichols, T. E. Statistical challenges in "big data" human neuroimaging. *Neuron* **97**, 263–268 (2018).
83. Fortin, J.-P. et al. Removing inter-subject technical variability in magnetic resonance imaging studies. *NeuroImage* **132**, 198–212 (2016).
84. Fortin, J.-P. et al. Harmonization of cortical thickness measurements across scanners and sites. *NeuroImage* **167**, 104–120 (2018).

Methods

GWAS participants and phenotypes. We performed GWAS separately on five publicly available datasets: the UKB (http://www.ukbiobank.ac.uk/resources/) study, the HCP (https://www.humanconnectome.org/) study, the PING (http://www.chd.ucsd.edu/research/ping-study.html) study, the PNC (https://www.ncbi.nlm.nih.gov/projects/gap/cgi-bin/study.cgi?study_id=phs000607.v1.p1) study and the ADNI (http://adni.loni.usc.edu/data-samples/) study. The main GWAS made use of data for 19,629 individuals of British ancestry from the UKB study, and the four other GWAS were performed on individuals of European ancestry (see Supplementary Table 29 for a summary of sample size of each GWAS).

The raw MRI, covariates and genetic data were downloaded from each data resource. We processed the MRI data locally using consistent procedures via advanced normalization tools (http://stnava.github.io/ANTs/) to generate ROI volume phenotypes for each dataset. The processing steps are detailed in the Supplementary Note, and we removed three ROIs (X5th ventricle and left/right lesion) with missing rates >99%. For each phenotype and continuous covariate variable, we further removed values greater than five times the median absolute deviation from the median value. All individuals were aged between 3 and 92 years. More information about study cohorts can be found in Supplementary Table 30 and the Supplementary Note.

Heritability estimation and genome-wide association analysis. We estimated the proportion of variation explained by all autosomal genetic variants in UKB using GCTA-GREML analysis[85] (http://cnsgenomics.com/software/gcta/). The adjusted covariates included age (at imaging), age-squared, sex, age–sex interaction, age-squared–sex interaction, TBV (for ROIs other than TBV itself), and the top 40 genetic principal components provided by UKB[86] (Data-Field 22009). The heritability estimates were tested in one-sided likelihood ratio tests. For genetic variants of autosomes, we performed association analysis for each ROI volume using PLINK[87] (https://www.cog-genomics.org/plink2/). The same set of covariates as in GCTA-GREML analysis were adjusted. The marginal genetic effects were tested in two-sided *t*-tests. GWAS were also separately performed on PING, PNC, ADNI and HCP data. In these four datasets, we adjusted for age, age-squared, sex, age–sex interaction, age-squared–sex interaction, TBV (for ROIs other than TBV itself), and top ten genetic principal components estimated from the genetic variants. We also adjusted for Alzheimer's disease status in ADNI GWAS. To examine the genetic correlation between UKB phase 1 and phase 2 data, we performed GWAS separately on data for the two phases. For genetic variants on the X chromosome, we performed association analysis using XWAS[88] (version 3.0, http://keinanlab.cb.bscb.cornell.edu/content/xwas/). We coded male genotypes on the X chromosome as 0/2, and sex was considered as a covariant in the model.

Genomic risk loci characterization and comparison with previous findings. Genomic risk loci were defined using the FUMA online platform (version 1.3.4, http://fuma.ctglab.nl/). We input the UKB GWAS summary statistics obtained from PLINK. FUMA first identified independent significant variants, which were defined as variants with a *P* value smaller than the predefined threshold and independent of other significant variants at $r^2 < 0.6$. Using these independent significant variants, FUMA then constructed LD blocks for independent significant variants by tagging all variants that had a minor allele frequency of ≥0.0005 and were in LD ($r^2 \geq 0.6$) with at least one of the independent significant variants. These variants included those from the 1000 Genomes reference panel and may not have been included in the present study. Based on these independent significant variants, (independent) lead variants were also identified as those that were independent from each other ($r^2 < 0.1$). If LD blocks of independent significant variants were closed (<250 kilobases based on the closest boundary variants of LD blocks), they were merged to a single genomic locus. Thus, each genomic locus could contain more than one independent significant variant and lead variant. Independent significant variants and all of the tagged variants were subsequently searched by FUMA in the NHGRI-EBI GWAS catalog (version 2019-01-31, https://www.ebi.ac.uk/gwas/) to look for their reported associations ($P < 9 \times 10^{-6}$) with any traits.

Gene-based association analysis and functional annotation. Gene-based association analysis was carried out for 18,796 protein-coding genes using MAGMA (v1.07, https://ctg.cncr.nl/software/magma/), which was also implemented in FUMA. Genetic variants were mapped according to their psychical positions, and then the gene-based *P* values were calculated by the GWAS summary statistics of mapped variants. Default MAGMA parameters were used, which mapped genetic variants to genes with no window around genes (window size = 0). In functional annotation and mapping analysis, variant-level signals were annotated with their biological functionality and then were linked to genes by a combination of positional, eQTL and three-dimensional chromatin interaction mappings. Specifically, independent significant variants and all of the tagged variants were first annotated for functional consequences on gene functions (for example, intergenic, intronic and exonic) using ANNOVAR[89] (version 2017-01-11). Functionally annotated variants were then mapped to 35,808 candidate genes based on physical position on the genome (tissue/cell types for 15-core chromatin state: brain), eQTL associations (tissue types: GTEx[90] v7 brain, BRAINEAC[91] and CommonMind Consortium[92]) and chromatin interaction mapping (built-in chromatin interaction data: dorsolateral prefrontal cortex, hippocampus[93]; annotate enhancer/promoter regions: E053-E082 brain[94]). We used default values for all other parameters.

For the detected genes, we performed lookups in the NHGRI-EBI GWAS catalog (version 2019-05-03) again to explore the previously reported associations with the same or other traits. We focused on traits including cognitive functions (such as general cognitive ability, cognitive performance and empathy quotient), intelligence, educational attainment, math ability (such as highest math class taken and self-reported math ability), reaction time, neuroticism, neurodegenerative diseases (such as Alzheimer's disease and Parkinson's disease) and neuropsychiatric disorders (such as major depressive disorder, schizophrenia and bipolar disorder).

Biological annotation and enrichment analyses. For the 14 brain tissues (GTEx[90] v7), we performed gene property analysis via MAGMA. That is, for each candidate gene, we tested whether its tissue-specific expression levels can be linked to the strength of its association with ROI volumes. We also performed cell-type/tissue-specific chromatin-based annotation analysis using stratified LDSC (https://github.com/bulik/ldsc/wiki/Cell-type-specific-analyses). The cell-type/tissue-specific annotations of DNase I hypersensitivity and activating histone marks (H3K27ac, H3K4me3, H3K4me1, H3K9ac and H3K36me3) were from the Roadmap Epigenomics consortium[94] and the ENCODE project[95]. For each annotation, we tested whether it had an enriched contribution to per-SNP heritability, conditional on the other annotations. DEPICT (version 1 rel194, https://github.com/perslab/depict) and MAGMA gene set analyses were used to explore the implicated biological pathway by the UKB GWAS summary statistics. Specifically, DEPICT tested 10,968 reconstituted gene sets, and the GWAS summary statistics with $P < 10^{-5}$ were used as input. The MAGMA gene set analysis examined 10,678 gene sets from the Molecular Signatures Database[96] (MSigDB, v6.2, http://software.broadinstitute.org/gsea/msigdb), including 4,761 curated gene sets and 5,917 Gene Ontology terms. All parameters in these analyses were set as default.

Meta-analysis of GWAS results. We meta-analyzed the UKB, PING, PNC, ADNI and HCP GWAS summary results using METAL (https://genome.sph.umich.edu/wiki/METAL) with the sample-size-weighted approach. Since the sample sizes of the four other datasets were small, we removed the variants that were not presented in the UKB data.

Genetic correlation estimation with LDSC. LD Hub (v1.9.1, http://ldsc.broadinstitute.org/ldhub/) was used to estimate the genetic correlation between several UKB ROI volumes and their corresponding traits studied in the ENIGMA consortium (http://enigma.ini.usc.edu/). The LDSC software (v1.0.0, https://github.com/bulik/ldsc) was then used to estimate the pairwise genetic correlation with 50 sets of collected GWAS summary statistics. In addition, for each ROI, we also examined the genetic correlation between its regional volumes collected in UKB phases 1 and 2. We used the pre-calculated LD scores provided by LDSC (https://data.broadinstitute.org/alkesgroup/LDSCORE/), which were computed using 1000 Genomes European data. We used HapMap3 (ref. [97]) variants and removed all variants in the major histocompatibility complex region.

Polygenic scoring. Polygenic profiles were created to examine the out-of-sample prediction power of the GWAS results. Specifically, we used PLINK to generate risk scores in testing data by summarizing across variants, weighed by their effect sizes estimated from training data. To account for the LD structure, two procedures were used: LD-based pruning (window size 50, step 5, $r^2 = 0.2$); and posterior effect size estimation under continuous shrinkage priors with an external LD reference panel[98] (https://github.com/getian107/PRScs). We tried five *P*-value thresholds for predictor selection in each of the two procedures: 1, 0.5, 0.05, 5×10^{-4} and 5×10^{-8}. Thus, ten polygenic profiles were generated for each ROI volume, and we reported the best prediction power that can be achieved by a single profile of the ten. The association between polygenic profile and phenotype was estimated and tested in a linear regression model, adjusting for the effects of age and sex. The additional phenotypic variation that can be explained by polygenic profile (that is, the incremental R-squared) was used to measure the prediction power.

For the UKB dataset, we randomly divided the 19,629 UKB individuals into ten folds, then used nine of these folds as training data to rerun GWAS, and created polygenic profiles on the individuals in the remaining fold, which served as testing data. We repeated this procedure ten times such that each fold alternated to serve as the testing data for exactly one time. We examined seven ROIs including the thalamus proper, caudate, putamen, pallidum, hippocampus, accumbens area and TBV. For the first six ROIs, their volumes were the sum of the volumes of the corresponding left and right ROIs. We then used these ROI-derived profiles to predict four brain-related traits: education (Data-Field: 845), reaction time (Data-Field: 20023), numeric memory (Data-Field: 4282) and fluid intelligence (Data-Field: 20016). We first assessed the cross-trait prediction ability of each profile, and then we selected the best profile for each ROI and put the seven profiles together in one model for multivariate analysis.

Next, we used the UKB GWAS results to perform prediction on ADNI, PING, PNC and HCP data for all 101 ROI volumes. The prediction accuracy was

evaluated on all samples in the four testing sets (with phenotype and genetic data available), not limited to individuals of European ancestry used in GWAS.

Reporting Summary. Further information on research design is available in the Nature Research Reporting Summary linked to this article.

Data availability

The data used in this work were obtained from five publicly available datasets: the UKB study, the HCP study, the PING study, the PNC study and the ADNI study. We used 50 sets of publicly available GWAS summary statistics from several GWAS databases. The data resources are summarized in Supplementary Table 24. All UKB and meta-analysis GWAS summary statistics of 101 ROI volumes can be found at https://github.com/BIG-S2/GWAS.

Code availability

We made use of publicly available software and tools. All codes used to generate results that are reported in this paper are available upon request.

References

85. Yang, J., Lee, S. H., Goddard, M. E. & Visscher, P. M. GCTA: a tool for genome-wide complex trait analysis. *Am. J. Hum. Genet.* **88**, 76–82 (2011).
86. Bycroft, C. et al. The UK Biobank resource with deep phenotyping and genomic data. *Nature* **562**, 203–209 (2018).
87. Purcell, S. et al. PLINK: a tool set for whole-genome association and population-based linkage analyses. *Am. J. Hum. Genet.* **81**, 559–575 (2007).
88. Gao, F. et al. XWAS: a software toolset for genetic data analysis and association studies of the X chromosome. *J. Heredity* **106**, 666–671 (2015).
89. Wang, K., Li, M. & Hakonarson, H. ANNOVAR: functional annotation of genetic variants from high-throughput sequencing data. *Nucleic Acids Res.* **38**, e164–e164 (2010).
90. GTEx Consortium The genotype-tissue expression (GTEx) pilot analysis: multitissue gene regulation in humans. *Science* **348**, 648–660 (2015).
91. Ramasamy, A. et al. Genetic variability in the regulation of gene expression in ten regions of the human brain. *Nat. Neurosci.* **17**, 1418–1428 (2014).
92. Fromer, M. et al. Gene expression elucidates functional impact of polygenic risk for schizophrenia. *Nat. Neurosci.* **19**, 1442–1453 (2016).
93. Schmitt, A. D. et al. A compendium of chromatin contact maps reveals spatially active regions in the human genome. *Cell Rep.* **17**, 2042–2059 (2016).
94. Roadmap Epigenomics Consortium et al. Integrative analysis of 111 reference human epigenomes. *Nature* **518**, 317–330 (2015).
95. ENCODE Project Consortium An integrated encyclopedia of DNA elements in the human genome. *Nature* **489**, 57–74 (2012).
96. Liberzon, A. et al. Molecular signatures database (MSigDB) 3.0. *Bioinformatics* **27**, 1739–1740 (2011).
97. International HapMap 3 Consortium Integrating common and rare genetic variation in diverse human populations. *Nature* **467**, 52–58 (2010).
98. Ge, T., Chen, C.-Y., Ni, Y., Feng, Y.-C. A. & Smoller, J. W. Polygenic prediction via Bayesian regression and continuous shrinkage priors. *Nat. Commun.* **10**, 1776 (2019).

Acknowledgements

This research was partially supported by US National Institutes of Health (NIH) grants MH086633 (H.Z.) and MH116527 (T.Li), and a grant from the Cancer Prevention Research Institute of Texas (H.Z.). We thank the individuals represented in the UKB, ADNI, HCP, PING and PNC datasets for their participation and the research teams for their work in collecting, processing and disseminating these datasets for analysis. This research has been conducted using the UKB resource (application number 22783), subject to a data transfer agreement. We gratefully acknowledge all of the studies and databases that made GWAS summary data available. Part of data collection and sharing for this project was funded by the ADNI (NIH grant U01 AG024904) and DOD ADNI (Department of Defense award number W81XWH-12-2-0012). ADNI is funded by the National Institute on Aging, the National Institute of Biomedical Imaging and Bioengineering and through generous contributions from the following: Alzheimer's Association; Alzheimer's Drug Discovery Foundation; Araclon Biotech; BioClinica; Biogen Idec; Bristol-Myers Squibb; Eisai; Elan Pharmaceuticals; Eli Lilly and Company; EuroImmun; Roche and its affiliated company Genentech; Fujirebio; GE Healthcare; IXICO; Janssen Alzheimer Immunotherapy Research and Development; Johnson and Johnson Pharmaceutical Research and Development; Medpace.; Merck and Co.; Meso Scale Diagnostics; NeuroRx Research; Neurotrack Technologies; Novartis Pharmaceuticals Corporation; Pfizer; Piramal Imaging; Servier; Synarc; and Takeda Pharmaceutical. The Canadian Institutes of Health Research is providing funds to support ADNI clinical sites in Canada. Private sector contributions are facilitated by the Foundation for the NIH (www.fnih.org). The grantee organization is the Northern California Institute for Research and Education, and the study is coordinated by the Alzheimer's Disease Cooperative Study at the University of California, San Diego. ADNI data are disseminated by the Laboratory for Neuro Imaging at the University of Southern California. Part of the data collection and sharing for this project was funded by the PING study (US NIH grant RC2DA029475). PING is funded by the National Institute on Drug Abuse and the Eunice Kennedy Shriver National Institute of Child Health and Human Development. PING data are disseminated by the PING Coordinating Center at the Center for Human Development, University of California, San Diego. Support for the collection of the PNC datasets was provided by grant RC2MH089983 awarded to R. Gur and RC2MH089924 awarded to H. Hakonarson. All PNC subjects were recruited through the Center for Applied Genomics at The Children's Hospital in Philadelphia. HCP data were provided by the HCP, WU-Minn Consortium (Principal Investigators: D. Van Essen and K. Ugurbil; 1U54MH091657) funded by the 16 NIH Institutes and Centers that support the NIH Blueprint for Neuroscience Research; and by the McDonnell Center for Systems Neuroscience at Washington University.

Author contributions

B.Z., H.Z. and Y.L. designed the study. B.Z. and T.Luo performed the experiments and analyzed the data. T.Li, J.Z., T.Luo, Y.S., X.W., L.Y., F.Z. and Z.Z. downloaded the datasets, preprocessed MRI and DNA data, and undertook the quantity controls. B.Z., H.Z. and Y.L. wrote the manuscript with feedback from all authors.

Competing interests

The authors declare no competing interests.

Additional information

Supplementary information is available for this paper at https://doi.org/10.1038/s41588-019-0516-6.

Correspondence and requests for materials should be addressed to H.Z.

nature research

Corresponding author(s): Hongtu Zhu

Last updated by author(s): 08/22/2019

Reporting Summary

Nature Research wishes to improve the reproducibility of the work that we publish. This form provides structure for consistency and transparency in reporting. For further information on Nature Research policies, see Authors & Referees and the Editorial Policy Checklist.

Statistics

For all statistical analyses, confirm that the following items are present in the figure legend, table legend, main text, or Methods section.

n/a	Confirmed
☐	☒ The exact sample size (*n*) for each experimental group/condition, given as a discrete number and unit of measurement
☐	☒ A statement on whether measurements were taken from distinct samples or whether the same sample was measured repeatedly
☐	☒ The statistical test(s) used AND whether they are one- or two-sided *Only common tests should be described solely by name; describe more complex techniques in the Methods section.*
☐	☒ A description of all covariates tested
☐	☒ A description of any assumptions or corrections, such as tests of normality and adjustment for multiple comparisons
☐	☒ A full description of the statistical parameters including central tendency (e.g. means) or other basic estimates (e.g. regression coefficient) AND variation (e.g. standard deviation) or associated estimates of uncertainty (e.g. confidence intervals)
☐	☒ For null hypothesis testing, the test statistic (e.g. *F*, *t*, *r*) with confidence intervals, effect sizes, degrees of freedom and *P* value noted *Give P values as exact values whenever suitable.*
☐	☒ For Bayesian analysis, information on the choice of priors and Markov chain Monte Carlo settings
☐	☒ For hierarchical and complex designs, identification of the appropriate level for tests and full reporting of outcomes
☐	☒ Estimates of effect sizes (e.g. Cohen's *d*, Pearson's *r*), indicating how they were calculated

Our web collection on statistics for biologists contains articles on many of the points above.

Software and code

Policy information about availability of computer code

Data collection

There is no clear distinction between software/code used for data collection vs data analysis, thus we list all software here:

ANTs v2.1.0 and v2.2.0, http://stnava.github.io/ANTs/;
PLINK v1.90 beta, https://www.cog-genomics.org/plink2/;
GCTA v1.91.7beta, http://cnsgenomics.com/software/gcta/;
METAL v2011-03-25, https://genome.sph.umich.edu/wiki/METAL;
FUMA v1.3.4, http://fuma.ctglab.nl/;
MGAMA v1.07, https://ctg.cncr.nl/software/magma;
LD Score Regression v1.0.0, https://github.com/bulik/ldsc/;
LD Hub v1.9.1, http://ldsc.broadinstitute.org/ldhub/;
XWAS v3.0, http://keinanlab.cb.bscb.cornell.edu/content/xwas;
DEPICT v1 rel194, https://github.com/perslab/depict;
PRScs v2019-05-15, https://github.com/getian107/PRScs;
MSigDB v6.2, http://software.broadinstitute.org/gsea/msigdb;
MaCH-Admix v2.0.203, http://www.unc.edu/~yunmli/MaCH-Admix ;
NHGRI-EBI GWAS Catalog v2019-01-31, https://www.ebi.ac.uk/gwas/home/;
The atlas of GWAS Summary Statistics v20190131, http://atlas.ctglab.nl/ (for genetic variants);
The atlas of GWAS Summary Statistics v20190503, http://atlas.ctglab.nl/ (for genes);
UK Biobank, http://www.ukbiobank.ac.uk/resources/;
PING, http://pingstudy.ucsd.edu/resources/genomics-core.html/;
PNC, https://www.ncbi.nlm.nih.gov/projects/gap/cgi-bin/study.cgi?study_id=phs000607.v1.p1/;
ADNI, http://adni.loni.usc.edu/data-samples/;
HCP, https://www.humanconnectome.org/.

Data analysis	Please see above.

For manuscripts utilizing custom algorithms or software that are central to the research but not yet described in published literature, software must be made available to editors/reviewers. We strongly encourage code deposition in a community repository (e.g. GitHub). See the Nature Research guidelines for submitting code & software for further information.

Data

Policy information about availability of data

All manuscripts must include a data availability statement. This statement should provide the following information, where applicable:

- Accession codes, unique identifiers, or web links for publicly available datasets
- A list of figures that have associated raw data
- A description of any restrictions on data availability

The data used in this work were obtained from five publicly available datasets: the UK Biobank (UKB) study, the Human Connectome Project (HCP) study, the Pediatric Imaging, Neurocognition, and Genetics (PING) study, the Philadelphia Neurodevelopmental Cohort (PNC) study, and the Alzheimer's Disease Neuroimaging Initiative (ADNI) study. This research has been conducted using the UK Biobank resource (application number 22783), subject to a data transfer agreement.
For UKB, the imputed genetic variants data was released in July 2017, and we used the imaging data of ~22,000 participants released until August 2018.
The raw MRI, covariates and genetic variants data were available from each data resource:
UK Biobank, http://www.ukbiobank.ac.uk/resources/;
PING, http://pingstudy.ucsd.edu/resources/genomics-core.html/;
PNC, https://www.ncbi.nlm.nih.gov/projects/gap/cgi-bin/study.cgi?study_id=phs000607.v1.p1/;
ADNI, http://adni.loni.usc.edu/data-samples/;
HCP, https://www.humanconnectome.org/.

We used 50 sets of publicly available GWAS summary statistics from several GWAS databases. The data resources are summarized in Supplementary Table 24.

The full set of UKB and meta-analysis GWAS summary statistics of ROI volumes are available at: https://med.sites.unc.edu/bigs2/data/gwas-summary-statistics/.

Field-specific reporting

Please select the one below that is the best fit for your research. If you are not sure, read the appropriate sections before making your selection.

☒ Life sciences ☐ Behavioural & social sciences ☐ Ecological, evolutionary & environmental sciences

For a reference copy of the document with all sections, see nature.com/documents/nr-reporting-summary-flat.pdf

Life sciences study design

All studies must disclose on these points even when the disclosure is negative.

Sample size	No power calculation was needed in advance. We used all samples passing standard quality controls (please see below). The sample size in current analysis was greater than that of most of the previous GWAS on brain volumetric phenotypes.
Data exclusions	The main GWAS made use of data of individuals of British ancestry (self-reported ethnic background, Data-Field 21000) from the UKB study, and the other four GWAS (PING, PNC, HCP, ADNI) were performed on individuals of European ancestry. For the imaging data, we removed three ROIs (X5th ventricle and left/right lesion) with missing rates > 99%. For each phenotype and continuous covariate variable, we further removed values greater than five times the median absolute deviation from the median value. For the genetic variants data, we performed standard quality controls on each dataset, including 1) exclude subjects with more than 10% missing genotypes; 2) exclude variants with minor allele frequency less than 0.01; 3) exclude variants with larger than 10% missing genotyping rate; 4) exclude variants that failed the Hardy-Weinberg test at 1*10^{-7} level; and 5) remove variants with imputation INFO score less than 0.8. For X chromosome analysis, the following X-specific quality control steps were performed: 1) variants on chromosomes other than X were removed, as well as variants in the pseudoau-tosomal regions (PARs) on X; 2) variants were removed if they had significantly different MAF between male and female (p-value <1.76*10^{-7}, Bonferroni-corrected). All the data exclusion criteria were pre-established.
Replication	The significant genetic variants discovered in the UKB sample were supported by a joint analysis with other four independent studies. We checked whether the variant effect signs were concordant in the five studies and whether the p-value of top UKB variants decreased after meta-analysis. Below are the main results of joint analysis: The joint analysis was carried out on 3,841,911 genetic variants which were present in all five sets of GWAS results. For the 7,310 significant associations, 63.8% (4,666) associations had the same effect signs across the five studies, and 97.0% (7,090) associations had the same effect signs in at least four studies (including UKB). 93.9% (1,877) of the top 2,000 significant associations had smaller p-value after meta-analysis, and 91.4% (6,678) of all the 7,310 associations were enhanced.
Randomization	All the five datasets are from observational studies, and we used all samples available after data exclusions listed above. Therefore, there is no equivalent process of randomization in the present analysis.

Blinding	The data are not from controlled randomized studies, thus there is no step equivalent to blinding involved.

Reporting for specific materials, systems and methods

We require information from authors about some types of materials, experimental systems and methods used in many studies. Here, indicate whether each material, system or method listed is relevant to your study. If you are not sure if a list item applies to your research, read the appropriate section before selecting a response.

Materials & experimental systems

n/a	Involved in the study
☒	☐ Antibodies
☒	☐ Eukaryotic cell lines
☒	☐ Palaeontology
☒	☐ Animals and other organisms
☐	☒ Human research participants
☒	☐ Clinical data

Methods

n/a	Involved in the study
☒	☐ ChIP-seq
☒	☐ Flow cytometry
☐	☒ MRI-based neuroimaging

Human research participants

Policy information about studies involving human research participants

Population characteristics	The main GWAS made use of data of individuals of British ancestry from the UKB study, and the other four GWAS were performed on individuals of European ancestry. The UKB genetic data has 8,944,375 genetic variants after genotyping quality controls, all individuals were ages between 40 and 80 with mean 62.51, the proportion of male is 0.47. More information about other study cohorts can be found in Supplementary Tables 29-30 and Supplementary Note.
Recruitment	Patients were recruited differently in each of the cohorts used, with some cohorts collected from general population and others from hospitals. Recruitment details and dataset overviews can be found in Sudlow et al. for UKB (https://doi.org/10.1371/journal.pmed.1001779), Satterthwaite et al. for PNC (https://doi.org/10.1016/j.neuroimage.2013.07.064), Weiner et al. for ADNI (https://doi.org/10.1016/j.jalz.2013.05.1769), and Jernigan et al. for PING (https://doi.org/10.1016/j.neuroimage.2015.04.057). The UKB significant variants were supported in the joint analysis and the UKB GWAS results had satisfactory prediction ability on four other independent cohorts suggesting that there was limited bias due to sample recruitment.
Ethics oversight	For UKB, the wide consultation, rigorous Ethics and Governance Framework, and Ethics and Governance Council oversight role have been essential in paving the way for UK Biobank to accomplish obtaining the multiple ethical and regulatory approvals required for participant recruitment, sample and data storage, linkages to routine health care data, enhancement studies, and the provision of access to data and samples for approved researchers. Substantial amounts of time, resources, patience, tenacity, and evidence of feasibility and/or acceptability from smaller scale pilot studies have also been required to provide regulatory bodies with the reassurance that they need of UK Biobank's rigorous approach and commitment to protecting the interests of its participants within an acceptable legal and ethical framework (details can be found in Sudlow et al. https://doi.org/10.1371/journal.pmed.1001779). More information about these study cohorts can be found in the above references in section "Recruitment", the acknowledgment of the main text, and the Supplementary Note.

Note that full information on the approval of the study protocol must also be provided in the manuscript.

Magnetic resonance imaging

Experimental design

Design type	Please see the Online Methods section for full details. This study made use of imaging data from Structural MRI and genetic variants data.
Design specifications	Details can be found in Miller et al. (https://doi:10.1038/nn.4393) and Alfaro-Almagro et al. (https://doi.org/10.1016/j.neuroimage.2017.10.034) for UKB, and Satterthwaite et al. for PNC (https://doi.org/10.1016/j.neuroimage.2013.07.064), Weiner et al. for ADNI (https://doi.org/10.1016/j.jalz.2013.05.1769), and Jernigan et al. for PING (https://doi.org/10.1016/j.neuroimage.2015.04.057). We then processed all the MRI data to generate imaging phenotypes using consistent procedures via advanced normalization tools (ANTs). The processing steps by ANTs were detailed in Tustison et al. (https://doi.org/10.1016/j.neuroimage.2014.05.044).
Behavioral performance measures	Behavioral performance measures were not used in this study.

Acquisition

Imaging type(s): Structural MRI.

Field strength: 3T in UKB, PNC, PING, and HCP; 1.5 T or 3T for ADNI.

Sequence & imaging parameters: Details can be found in Miller et al. (https://doi:10.1038/nn.4393) and Alfaro-Almagro et al. (https://doi.org/10.1016/j.neuroimage.2017.10.034) for UKB, and Satterthwaite et al. for PNC (https://doi.org/10.1016/j.neuroimage.2013.07.064), Weiner et al. for ADNI (https://doi.org/10.1016/j.jalz.2013.05.1769), and Jernigan et al. for PING (https://doi.org/10.1016/j.neuroimage.2015.04.057).

Area of acquisition: The whole brain scan was used.

Diffusion MRI ☐ Used ☒ Not used

Preprocessing

Preprocessing software: Details can be found in Miller et al. (https://doi:10.1038/nn.4393) and Alfaro-Almagro et al. (https://doi.org/10.1016/j.neuroimage.2017.10.034) for UKB, Satterthwaite et al. for PNC (https://doi.org/10.1016/j.neuroimage.2013.07.064), Weiner et al. for ADNI (https://doi.org/10.1016/j.jalz.2013.05.1769), and Jernigan et al. for PING (https://doi.org/10.1016/j.neuroimage.2015.04.057). The processing steps by ANTs were detailed in Tustison et al. (https://doi.org/10.1016/j.neuroimage.2014.05.044).

Normalization: Normalization/standardization using the ANTs software were detailed in Tustison et al. (https://doi.org/10.1016/j.neuroimage.2014.05.044) and Avants et al. (https://doi.org/10.1016/j.neuroimage.2010.09.025).

Normalization template: We use the OASIS-30 Atropos template for registration and Mindboggle-101 atlases for labeling. Details can be found in https://mindboggle.info/data.html, Klein and Tourville (https://doi.org/10.3389/fnins.2012.00171) and Tustison et al. (https://doi.org/10.1016/j.neuroimage.2014.05.044). The processing steps by ANTs were detailed in Tustison et al. (https://doi.org/10.1016/j.neuroimage.2014.05.044).

Noise and artifact removal: Noise and artifact removal from raw data can be found in Miller et al. (https://doi:10.1038/nn.4393) and Alfaro-Almagro et al. (https://doi.org/10.1016/j.neuroimage.2017.10.034) for UKB, Satterthwaite et al. for PNC (https://doi.org/10.1016/j.neuroimage.2013.07.064), Weiner et al. for ADNI (https://doi.org/10.1016/j.jalz.2013.05.1769), and Jernigan et al. for PING (https://doi.org/10.1016/j.neuroimage.2015.04.057). Further processing steps such as N4 bias correction by ANTs were detailed in Tustison et al. (https://doi.org/10.1016/j.neuroimage.2014.05.044).

Volume censoring: No volume censoring was used in processing structural images.

Statistical modeling & inference

Model type and settings: Statistical modeling was not used when generating imaging phenotypes. But within this study inference was applied at the level of the combined imaging-genetics modelling.

Effect(s) tested: Statistical modeling was not used when generating imaging phenotypes. But within this study inference was applied at the level of the combined imaging-genetics modelling.

Specify type of analysis: ☐ Whole brain ☐ ROI-based ☒ Both

Anatomical location(s): We use the OASIS-30 Atropos template for registration and Mindboggle-101 atlases for labeling. Details can be found in https://mindboggle.info/data.html, Klein and Tourville (https://doi.org/10.3389/fnins.2012.00171) and Tustison et al. (https://doi.org/10.1016/j.neuroimage.2014.05.044). The 101 brain region parcellation was performed by the Multi-Atlas joint label fusion using ANTs. The processing steps by ANTs were detailed in Tustison et al. (https://doi.org/10.1016/j.neuroimage.2014.05.044).

Statistic type for inference (See Eklund et al. 2016): Inference was not carried out when generating imaging phenotypes. But within this study inference was applied at the level of the combined imaging-genetics modelling.

Correction: Inference was not carried out when generating imaging phenotypes. But within this study inference was applied at the level of the combined imaging-genetics modelling.

Models & analysis

n/a	Involved in the study
☒	☐ Functional and/or effective connectivity
☒	☐ Graph analysis
☒	☐ Multivariate modeling or predictive analysis